Electronic Supplementary Material (ESI) for Journal of Materials Chemistry A.

Phosphorus dual-site driven CoS_2@S, N co-doped porous carbon nanosheets for flexible quasi-solid-state supercapacitors

Shude Liu,[1] Daqiang Gao,[2] Junfu Li,[2] Kwan San Hui,[3] Ying Yin,*, [1, 4] Kwun Nam Hui,*,[5] and Seong Chan Jun*,[1]

[1]School of Mechanical Engineering, Yonsei University, Seoul 120-749, South Korea.
[2]Key Laboratory for Magnetism and Magnetic Materials of MOE, Key Laboratory of Special Function Materials and Structure Design of MOE, Lanzhou University, Lanzhou, 730000, China.
[3]School of Mathematics, University of East Anglia, Norwich, NR4 7TJ, United Kingdom.
[4]Guangxi Key Laboratory of Information Materials, Guilin University of Electronic Technology, Guilin 541004, PR China.
[5]Institute of Applied Physics and Materials Engineering, University of Macau, Avenida da Universidade, Taipa, Macau, China.
*Corresponding author's E-mail: bizhui@umac.mo; yingguet@126.com; scj@yonsei.ac.kr

Experimental Section

Materials synthesis

Preparation of Co nanoparticles embedded in N-doped C (Co@N-C) on the CF substrate

Co−MOF nanosheet arrays were synthesized on the CF substrate according to a modified solution method.[1] In detail, 60 mL of an aqueous solution containing 24 mmol 2-methylimidazole ($C_4H_6N_2$) was quickly mixed with 60 mL of aqueous solution of $Co(NO_3)_2 \cdot 6H_2O$ (3 mmol). The obtained mixture and two pieces of cleaned CF substrate (2×4 cm^2) were kept for 5 h at approximately 15 °C. The products were collected, rinsed with distilled water several times, and dried at 70 °C for 12 h. The pyrolysis of Co−MOF was performed at 700 °C for 2 h with a heating rate of 5 °C min^{-1} under Ar/H_2 with 95: 5 flow ratio (150 sccm) atmospheres.

P-doped CoS_2 (P-CoS_2) embedded in P, S-doped N-C (P-CoS_2@P, S, N-C) matrix on the CF substrate

The sulfuration and phosphorization of Co@N-C on the CFs were conducted in a horizontal quartz tube furnace under Ar (100 sccm) atmosphere. Briefly, 0.12 g of Co@N-C powder and a piece of Co@N-C on the CF were placed in the middle of a porcelain boat, while 0.48 g of S powder was placed upstream of the tube furnace. The porcelain boat was placed in a tube furnace, heated from room temperature (~20 °C) to 350 °C with a ramp rate of 10 °C min^{-1}, and kept for 2 h under Ar to yield CoS_2@S, N-C/CF. The as-prepared CoS_2@S, N-C/CF (0.1 g powder) and a piece of CoS_2@S, N-C/CF were further phosphatized with 0.4 g of NaH_2PO_2 powder at the ventilation end of tube furnace under Ar (100 sccm), in which the temperature of the front zone was raised from 20°C to 300 °C for 1 h at a heating rate of 6 °C min^{-1}, and the temperature of the front zone was increased from 20 °C to 400 °C for 1 h at a heating rate of 4 °C min^{-1}. Finally, P-CoS_2@P, S, N-C/CF hybrid was produced.

Metallic Co embedded in the P, N doped-C (Co@P, N-C) matrix on the CF substrate

To prepare Co@P, N-C, the quartz boat with Co@N-C (0.1 g powder and a piece of

Co@N-C/CF) and $NaH_2PO_2 \cdot H_2O$ (0.2 g) were placed at two separate positions in the tube furnace, that is, Co@N-C was placed downstream and $NaH_2PO_2 \cdot H_2O$ upstream of the furnace. Phosphorization was conducted at 300 °C for 2 h with a heating rate of 2 °C min^{-1} under Ar atmosphere.

Material characterization

The as-synthesized samples were characterized by X-ray diffractometer (SmartLab, Rigaku) equipped with Cu Kα radiation (λ = 1.54 Å), field-emission scanning electron microscope (SEM; JSM-7800F, JEOL) coupled with an energy-dispersive X-ray spectroscope (EDS) analyzer, transmission electron microscope (TEM; JEM-F200, JEOL), X-ray photoelectron spectrometer (XPS; K-alpha, Thermo Fisher), nitrogen adsorption–desorption apparatus (Autosorb-iQ 2ST/MP, Quantachrome) using nitrogen as an adsorptive at 77 K, and a Raman spectrometer (LabRAM Aramis, Horiba Jobin Yvon).

Electrochemical measurements

Electrochemical measurements were conducted in a three-electrode configuration (Ivium Technologies, Netherlands) in a 2 M KOH aqueous solution. The prepared sample (1 cm×1 cm), Pt slice, and $Hg/HgCl_2$/saturated KCl (SCE) were employed as the working, counter, and reference electrodes, respectively. The average mass loadings of CoS_2@S, N-C, P-CoS_2@P, S, N-C, Co@N-C and (b) Co@P, N-C deposited on the CF substrate before and after deposition were 1.3, 1.4, 0.9 and 1.0 mg cm^{-2}, respectively. Electrical impedance spectroscopy (EIS) was performed in the frequency range from 0.01 Hz to 1 MHz with the amplitude of the sinusoidal voltage of 10 mV. The specific capacity (Q_c, mA h g^{-1}) of the P-doped CoS_2@P, S, N tri-doped carbon and the specific capacitance (C_a, F g^{-1}) of P, Co, N tri-doped C calculated from their corresponding galvanostatic charge–discharge (GCD) curves were expressed as follows:[2]

$$Q_c = 2\frac{\int_{0}^{\Delta t} V_s dt}{mU_s} \tag{1}$$

$$C_a = \frac{I\int_{t_i}^{t_f} V_s dt}{m\int_{V_s}^{0} V_p dV} \tag{2}$$

where I (A) is the discharge current density, m (g) is the mass of active materials, V_s (V) is the operating potential during discharge process, Δt (s) is the discharge time, U_s (V) is the potential window, and t_f (s) and t_i (s) are the final and initial nodes in the discharge process, respectively.

P-CoS_2@P, S, N-C as the positive electrode and P@P, S, N-C as the negative electrode were assembled together and separated by a piece of cellulose paper separator, with the poly(vinyl alcohol)/potassium hydroxide (PVA/KOH) gel electrolyte. PVA/KOH electrolyte was prepared by dissolving 4 g of PVA into 20 mL of DI water and then mixing with KOH (20 mL, 4 M) at 85 °C until a clear viscous solution was obtained under continuous stirring.[1] The optimized mass ratio of the positive electrode material to the negative electrode material was determined to be 0.16 according to the charge balance theory ($Q^+ = Q^-$) as follows:[1]

$$Q = m \times C \times V \tag{3}$$

$$Q_+ \times m_+ = C_- \times m_- \times V_- \tag{4}$$

where Q is the stored charge (C), m is the loading mass of active materials (g), C is the specific capacity (mAh g^{-1}), ΔV is the potential window (V), and the superscripts + and − represent the positive and negative electrodes, respectively.

The specific capacitance (C; F g^{-1}), energy density (E; Wh kg^{-1}), and power density (P; W kg^{-1}) were calculated as follows:[2]

$$C_R = 2\frac{I\int_0^{\Delta t} V_R dt}{MU_R} \tag{5}$$

$$E = \frac{I\int_0^{\Delta t} V_R dt}{3.6 \cdot M} \tag{6}$$

$$P = \frac{3600 \times E}{\Delta t} \tag{7}$$

where $M\ (g)$ is the total mass of active materials in both electrodes, V_R (V) is the operating voltage during discharge process, and U_R(V) is the voltage window.

Density functional theory (DFT) calculations

All DFT calculations were conducted using the Vienna ab initio simulation package (VASP).[3] Projector augmented wave (PAW) potentials were employed to consider the electron–ion interactions.[4] The exchange and correlation effects to relax the atomic structures were analyzed by the generalized gradient approximation with the Perdew-Burke-Ernzerhof (GGA-PBE) function.[5] The energy convergence threshold to obtain the wave functions was 10^{-5} eV, and ionic relaxations were conducted until all force components became <0.02 eV $Å^{-1}$. The cut-off energy of 400 eV and the Monkhorst-Pack K-points were considered for the Brillouin-zone integration to describe the plane-wave basis restriction. An optimized geometry with 2×2×1 supercell single layer was used to account for the electronic structure and OH^- adsorption. For the P-doped CoS_2, we used one P atom to replace one S atom. To avoid the interaction between two neighboring surfaces, we introduced a vacuum slab of 15 Å.[6]

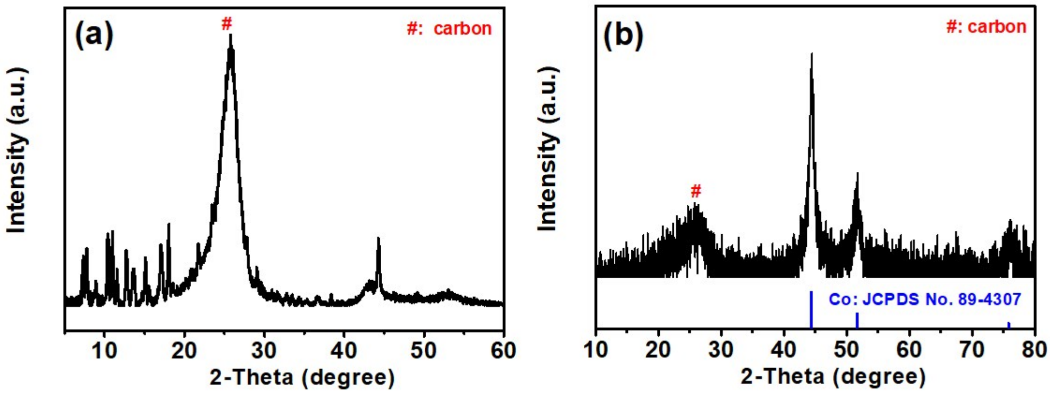

Fig. S1 XRD patterns of (a) Co-MOF and (b) Co@N-C nanosheets.

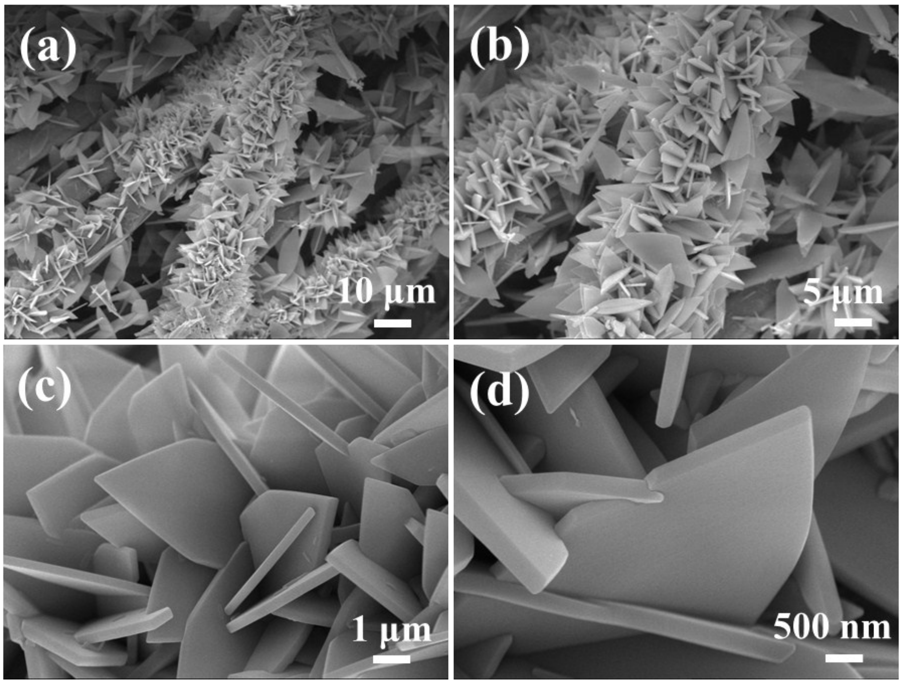

Fig. S2 (a–d) SEM images of the Co-MOF nanosheets.

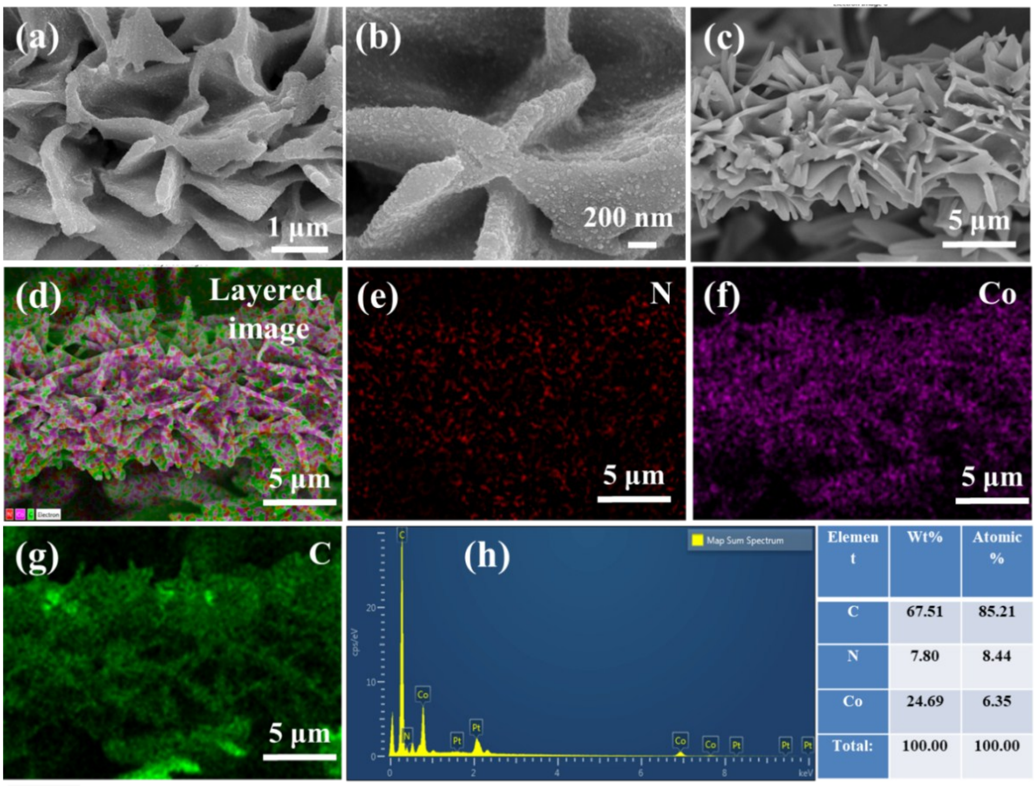

Element	Wt%	Atomic %
C	67.51	85.21
N	7.80	8.44
Co	24.69	6.35
Total:	100.00	100.00

Fig. S3 (a, b) SEM images, (c-g) SEM-EDS images, and (h) the EDS spectrum and the corresponding elemental content in the Co@N-C nanosheets.

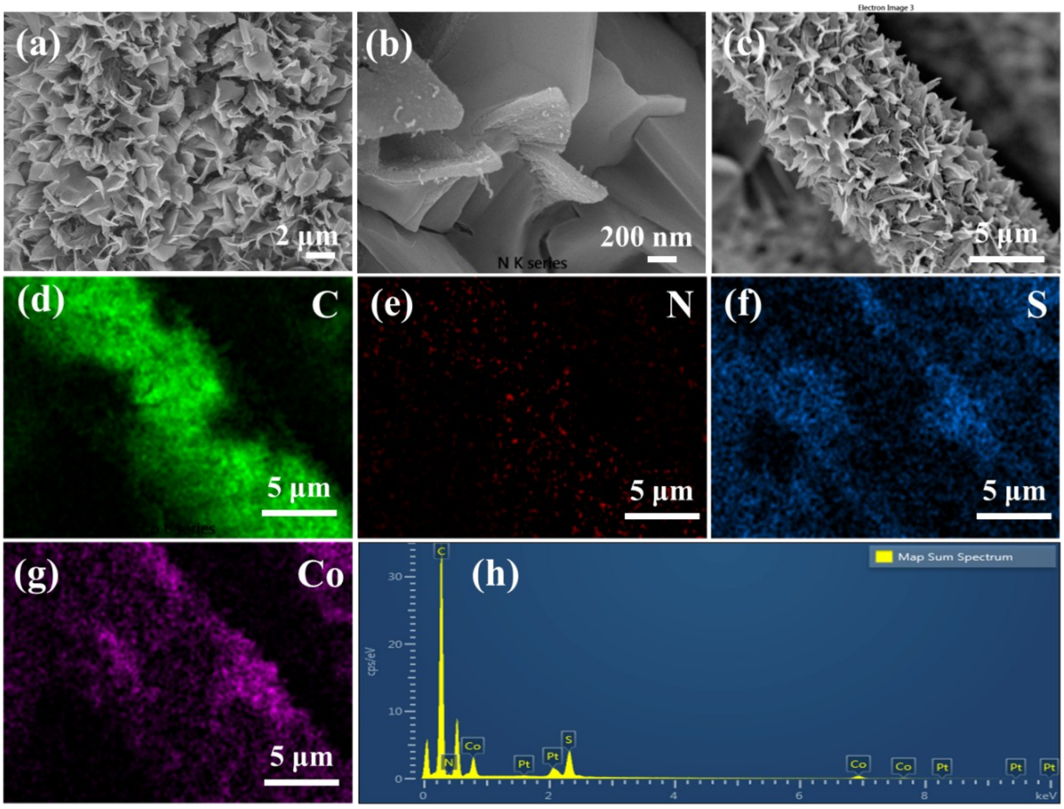

Fig. S4 (a, b) SEM image, (c–h) SEM-EDS images, and EDS spectrum in the CoS_2@S, N-C nanosheets.

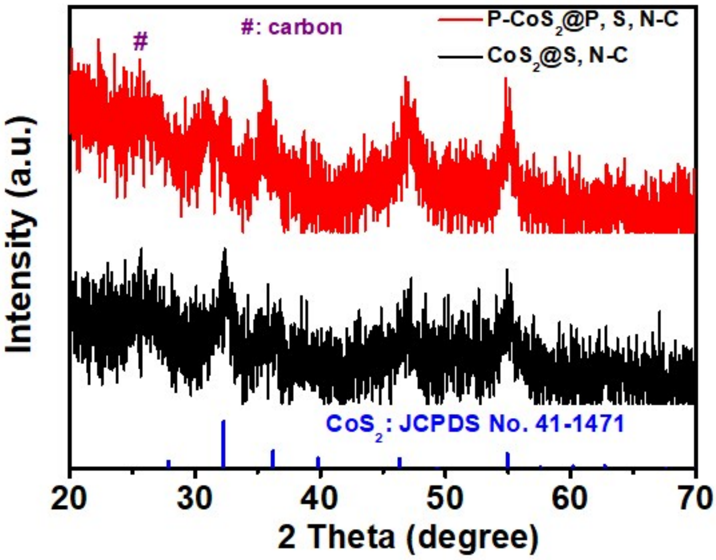

Fig. S5 XRD patterns of the CoS$_2$@S, N-C and P-CoS$_2$@P, S, N-C nanosheets.

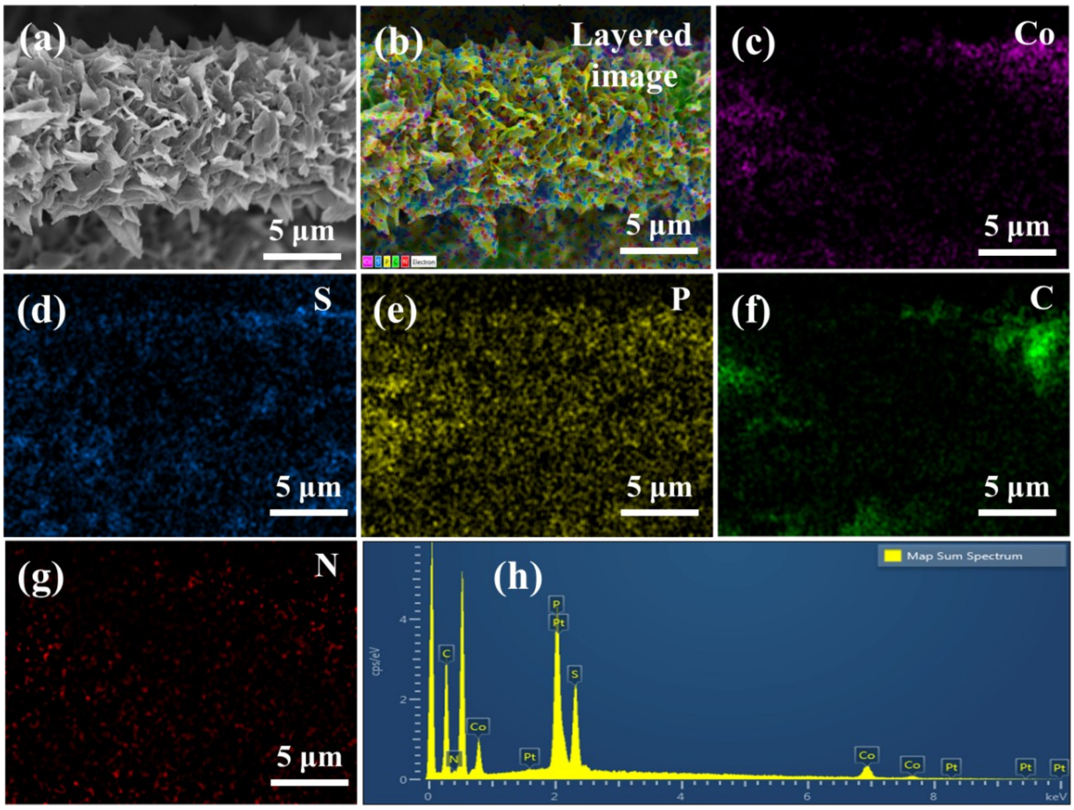

Fig. S6 (a) SEM image, (b–g) the corresponding elemental mappings, and (h) EDS spectrum and the corresponding elemental content in the P-CoS$_2$@P, S, N-C nanosheets.

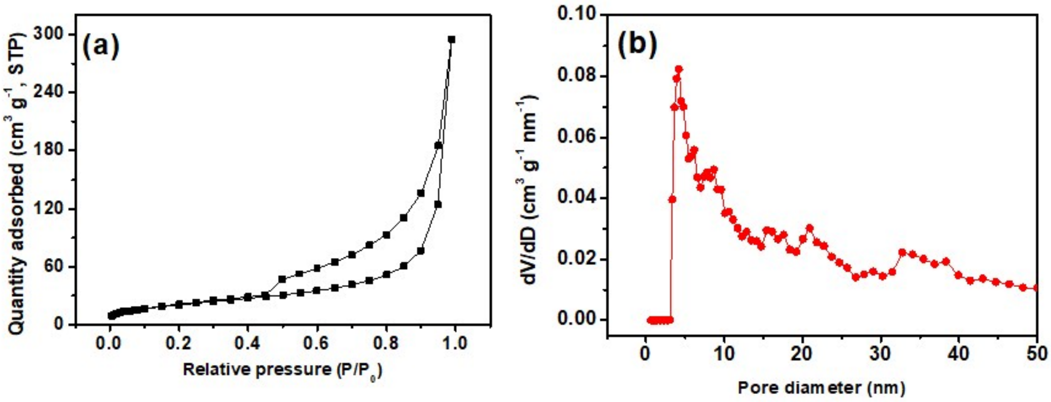

Fig. S7 Nitrogen adsorption–desorption isotherm and the corresponding pore size distribution plot of the P-CoS_2@P, S, N-C nanosheets.

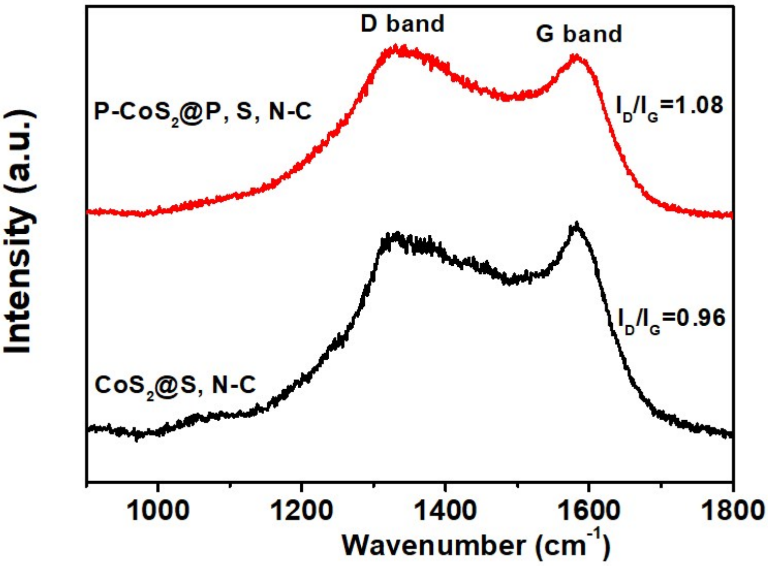

Fig. S8 Raman spectra of the CoS_2@S, N-C and P-CoS_2@P, S, N-C nanosheets.

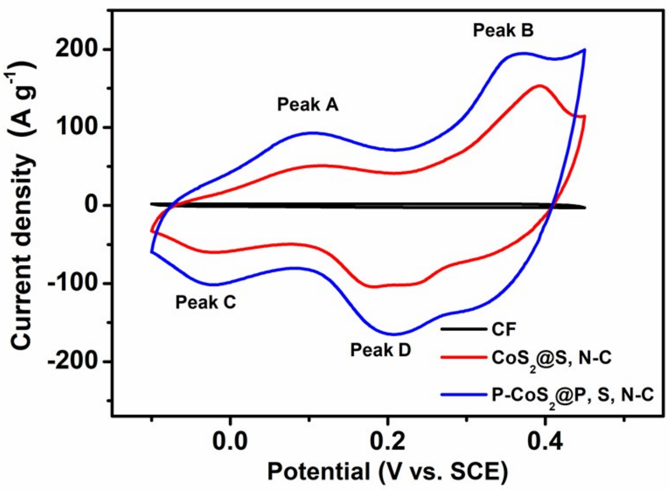

Fig. S9 Comparison of the CV curves of bare CF, CoS_2@S, N-C and P-CoS_2@P, S, N-C electrodes at a scan rate of 100 mV s^{-1}.

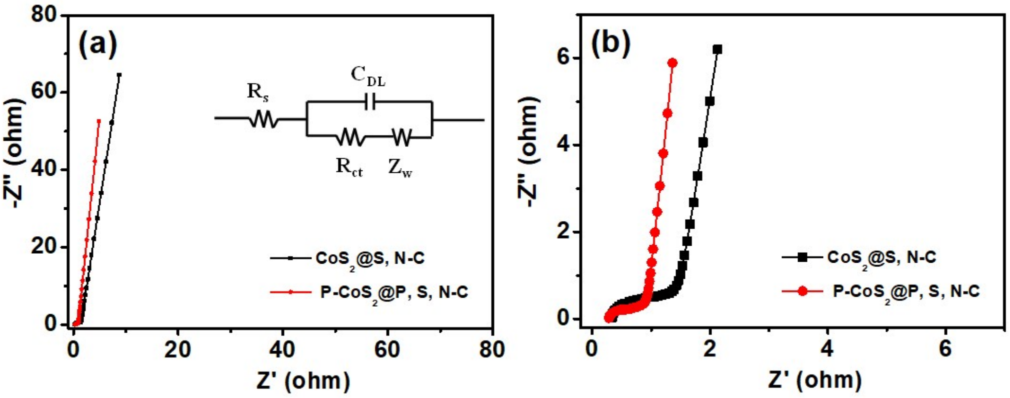

Fig. S10 EIS plots of the CoS_2@S, N-C and P-CoS_2@P, S, N-C electrodes at different magnifications.

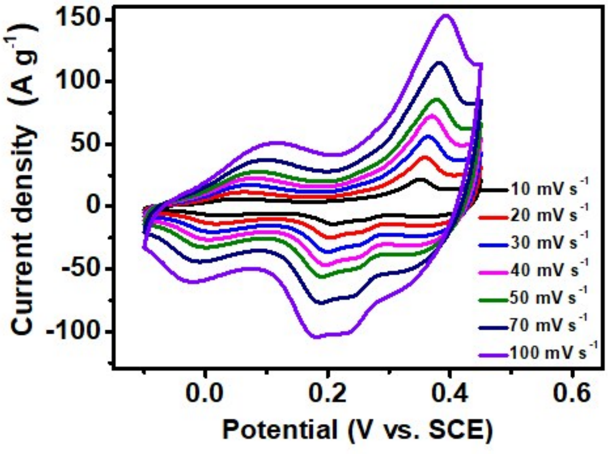

Fig. S11 CV curves of the CoS_2@S, N-C electrode at various scan rates.

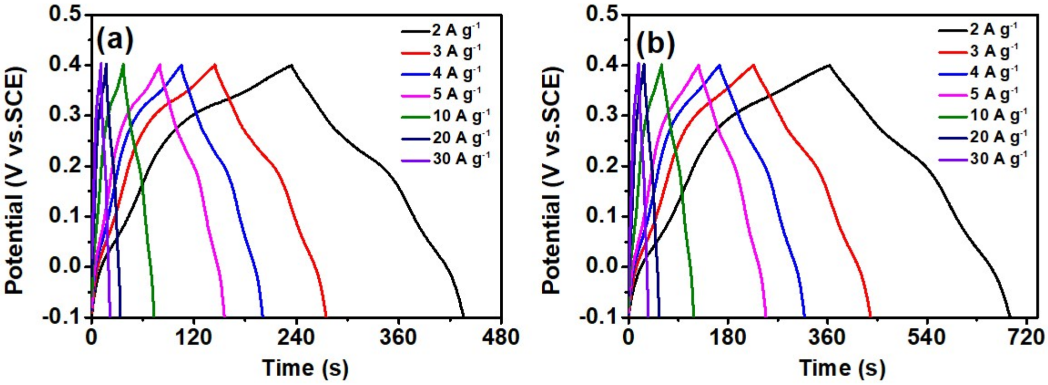

Fig. S12 GCD curves of the (c) CoS_2@S, N-C and (d) P-CoS_2@P, S, N-C electrodes at different current densities.

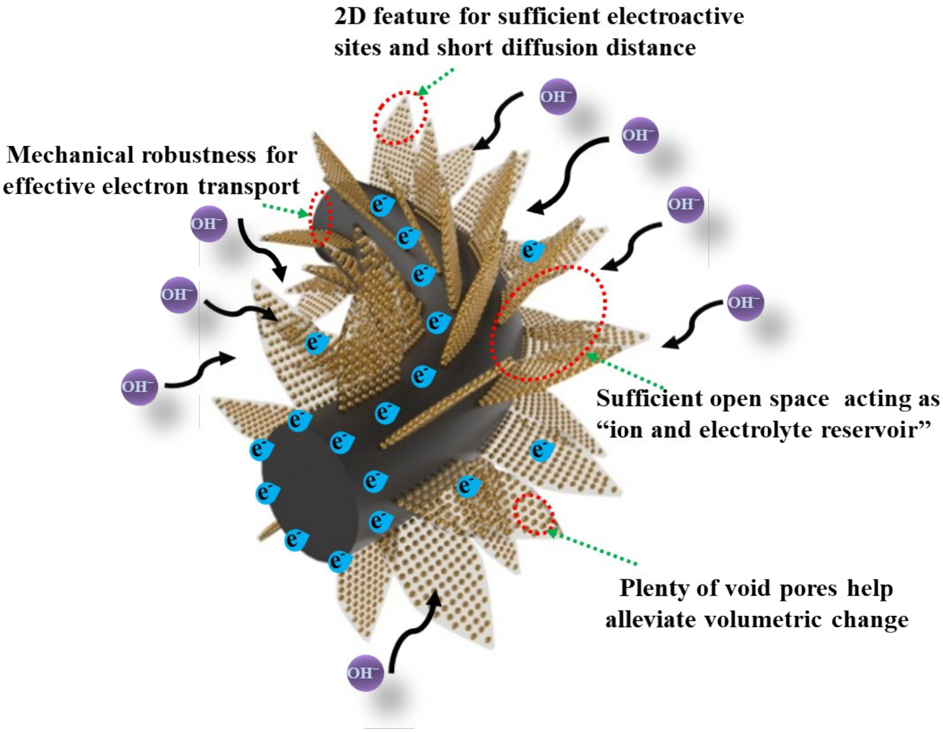

Fig. S13 Schematic showing the structural advantage of P-CoS_2@P, S, N-C for charge storage.

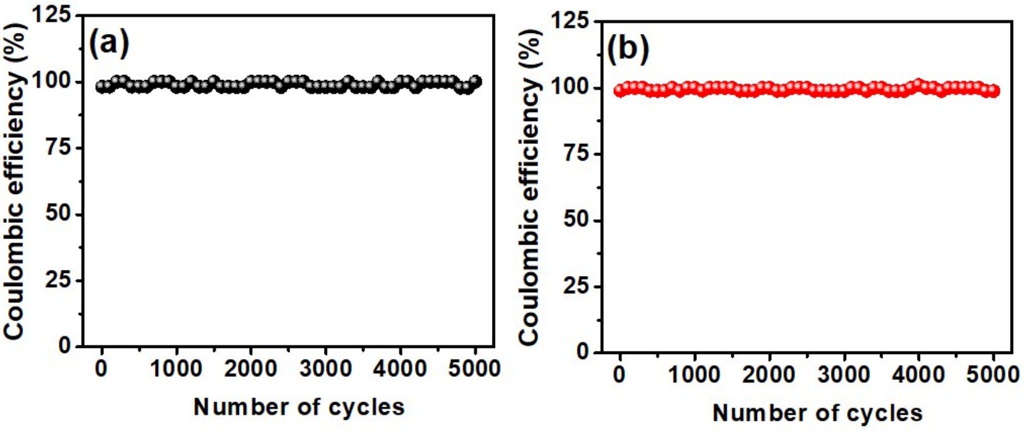

Fig. S14 Coulombic efficiencies of the (a) CoS_2@S, N-C and (b) P-CoS_2@P, S, N-C electrodes during cycling at a current density of 30 A g^{-1}.

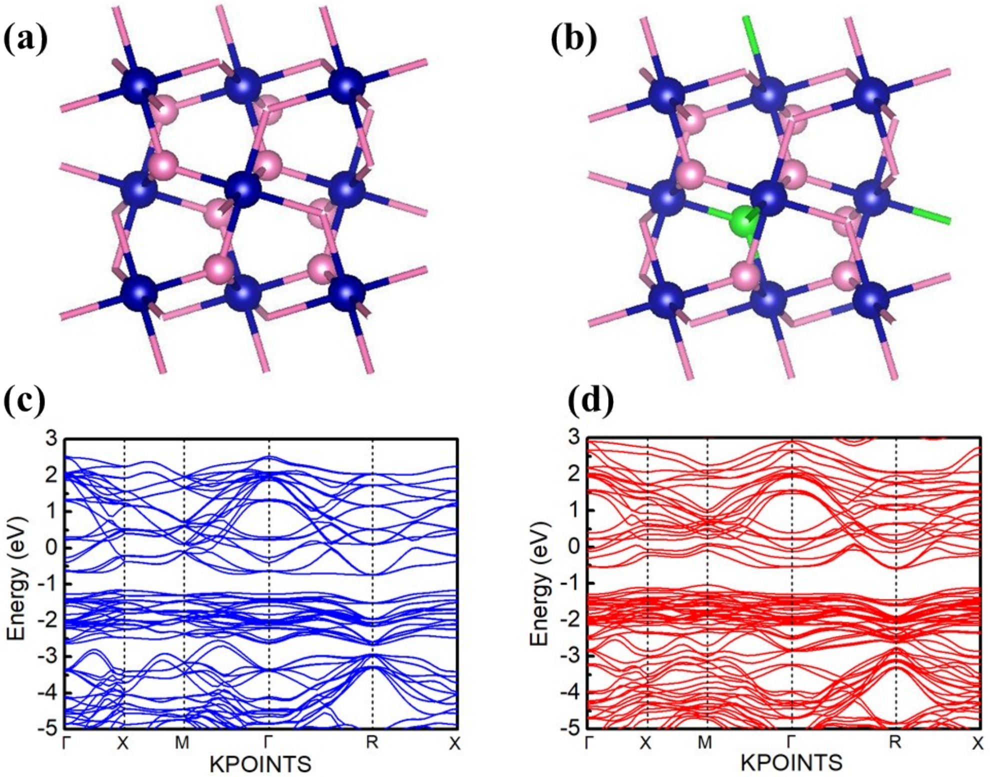

Fig. S15 Ball-and-stick models of the atomic structure of (a) CoS_2 and (b) P-CoS_2 systems (Co appears in blue, S in pink, and P in green). The electronic band structures of (c) CoS_2 and (d) P-CoS_2.

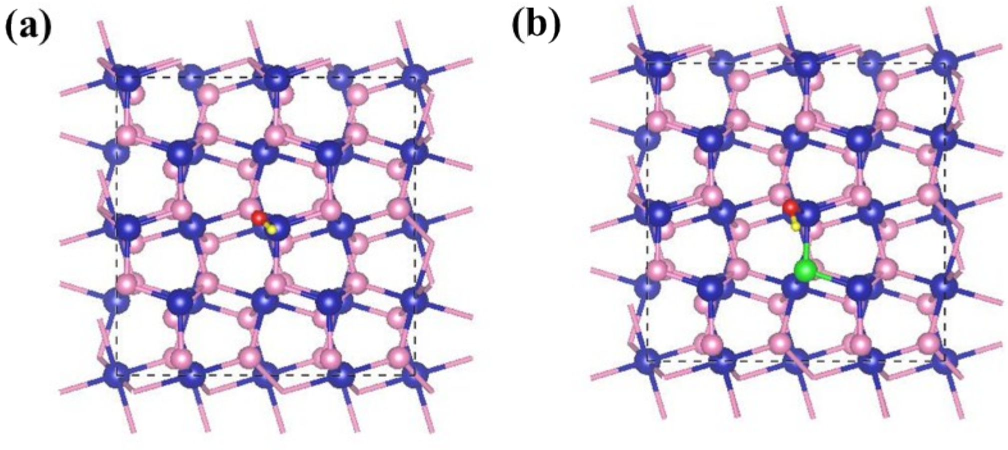

Fig. S16 Top views of the crystal structure on the Co sites in the (100) slab of (e) CoS_2 and (f) P-CoS_2. Co appears in blue, S in pink, P in green, O in red, and H in yellow.

The formation energy (E_f) and surface adsorption energy (E_{ads}) of OH^- of different systems were defined and calculated as follows:

$$E_f(CoS_2) = E(P\text{-}CoS_2) - E(CoS_2) + (\mu_P - \mu_S) \approx -0.825966\ \text{eV} \tag{8}$$

$$E_f(P\text{-}CoS_2) = E(OH\text{-}P\text{-}CoS_2) - E(OH\text{-}CoS_2) + (\mu_P - \mu_S) \approx -1.012996\ \text{eV} \tag{9}$$

where μ_P and μ_S are the chemical potentials of the P and S atoms, respectively, which can be approximately replaced by their corresponding single-point energy.

$$E_{ads}(CoS_2) = E(OH\text{-}CoS_2) - E(CoS_2) - E(OH^-) \approx -3.477933\ \text{eV} \tag{10}$$

$$E_{ads}(P\text{-}CoS_2) = E(OH\text{-}P\text{-}CoS_2) - E(P\text{-}CoS_2) - E(OH^-) \approx -3.664963\ \text{eV} \tag{11}$$

where $E(*\text{–}OH)$ is the total energy of CoS_2 and P-CoS_2 with OH^- adsorbed on the Co sites in (100) surface; $E(slab)$ is the total energy of (100) surface slab; and $E(OH^-)$ is the total energy of an isolated OH^-.

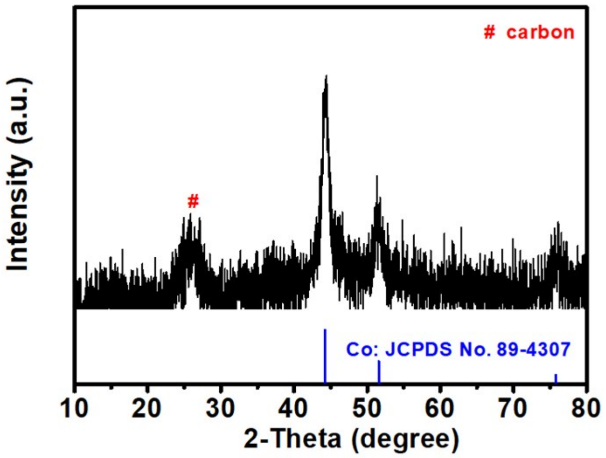

Fig. S17 XRD patterns of the Co@P, N-C nanosheets.

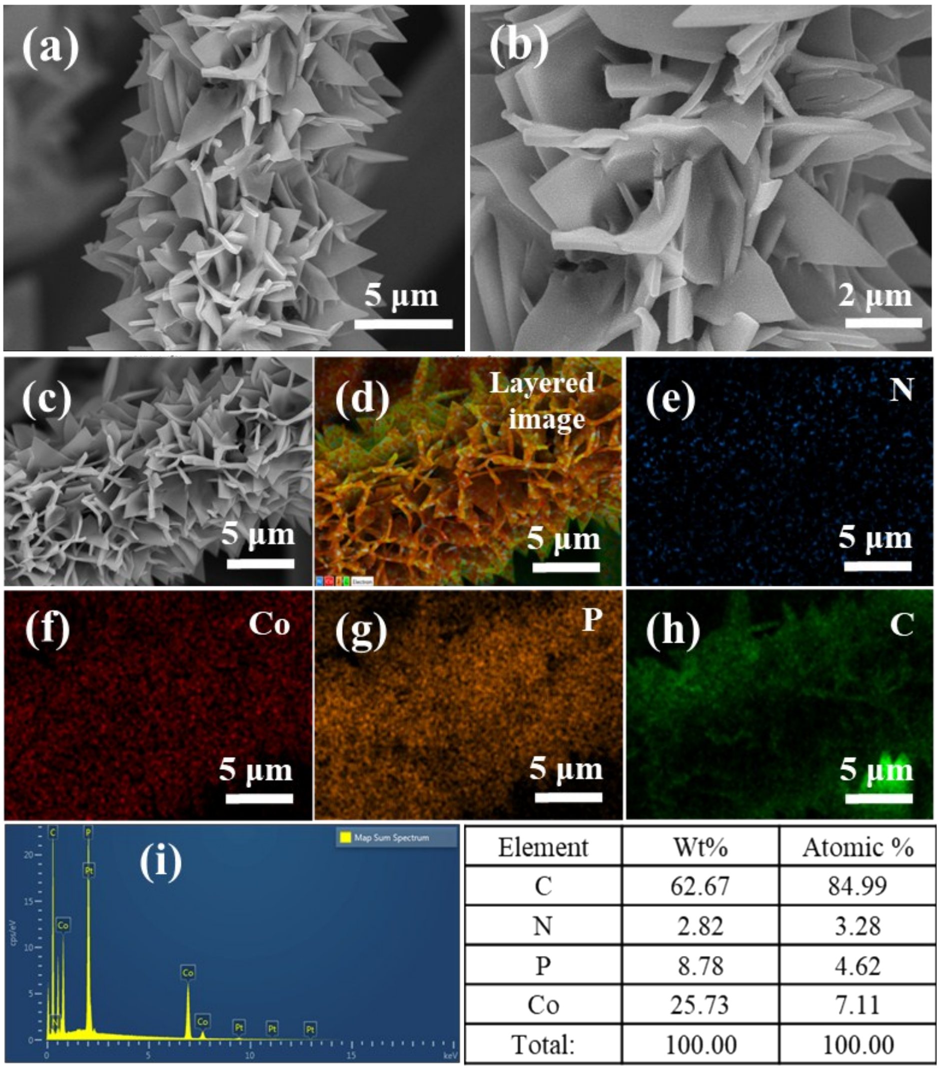

Element	Wt%	Atomic %
C	62.67	84.99
N	2.82	3.28
P	8.78	4.62
Co	25.73	7.11
Total:	100.00	100.00

Fig. S18 (a, b) SEM image, (c–i) SEM-EDS images, and EDS spectrum and the corresponding elemental content in the Co@P, N-C nanosheets.

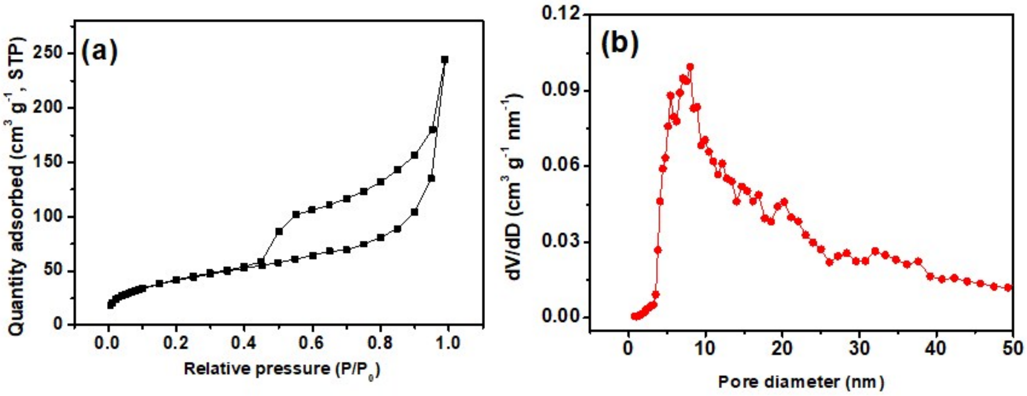

Fig. S19 Nitrogen adsorption–desorption isotherm and the corresponding pore size distribution plot of the Co@P, N-C nanosheets.

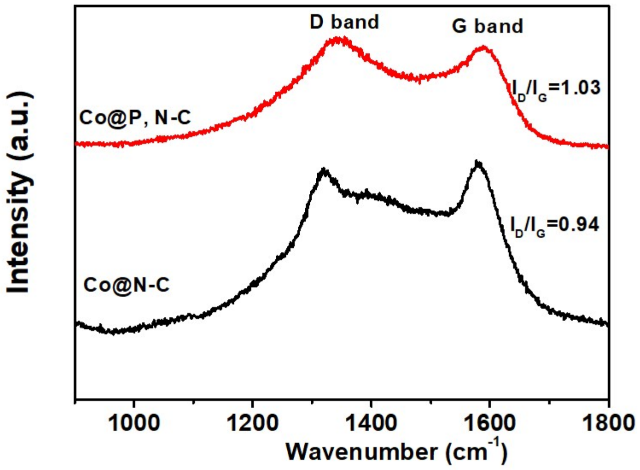

Fig. S20 Raman spectra of the Co@N-C and (b) Co@P, N-C nanosheets

The Raman spectra of Co@N-C and Co@P, N-C show two characteristic peaks at 1345 and 1585 cm^{-1}, which can be attributed to the D and G bands of the carbonaceous materials, respectively. Furthermore, the I_D/I_G value of Co@P, N-C (1.03) is larger than that of Co@N-C (0.94), indicating that the phosphatization treatment facilitates the production of defective sites.

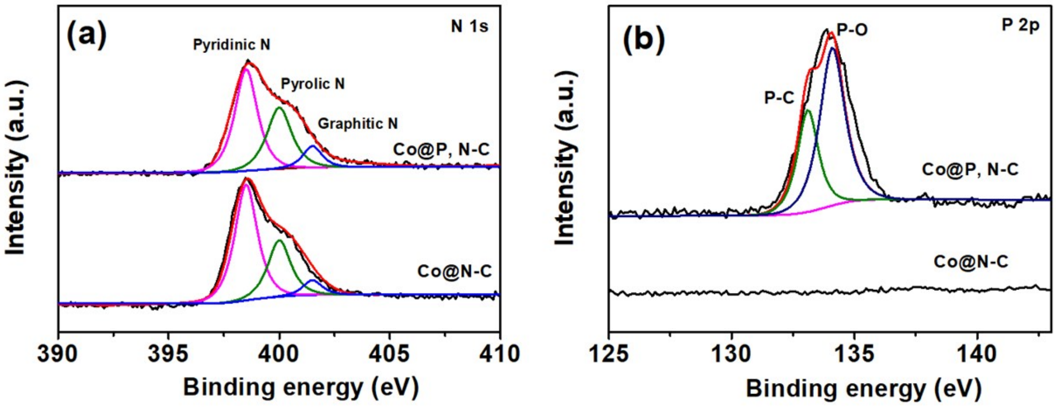

Fig. S21 High-resolution X-ray photoelectron spectra of (a) N 1s and (b) P 2p for the Co@N-C and (b) Co@P, N-C nanosheets.

The chemical states of the N and P atoms in Co@P, N-C were then analyzed by XPS. The X-ray photoelectron N 1s spectra consist of three components at approximately 398.5, 400.0, and 401.5 eV, corresponding to pyridinic N, pyrrolic N, and graphitic N, respectively.[7] In the XPS P 2p spectrum, the component peak centered at approximately 132.1 eV can be assigned to the P−C bond, while that at approximately 134.0 eV indicates the existence of the P−O bond. These results demonstrate that the N and P atoms have been successfully incorporated into the carbon matrixes. Doping covalent heteroatom would favor the tuning of the surface charge and defect distribution of C, which is responsible for the enhanced electrochemical activity.[8]

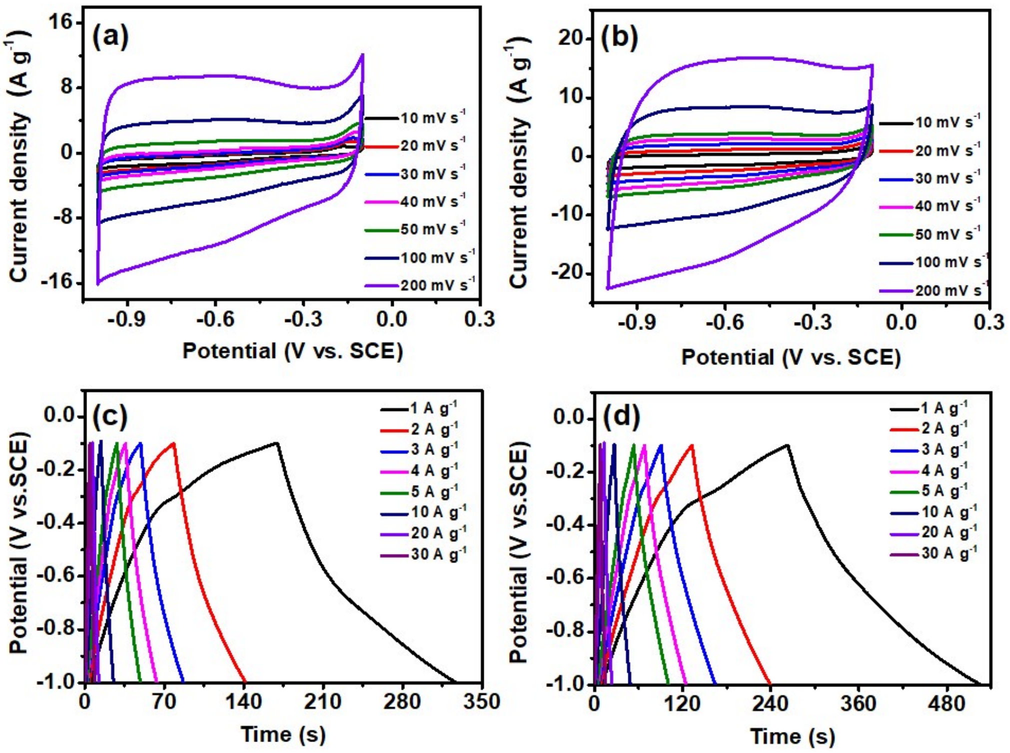

Fig. S22 CV curves of (a) Co@N-C and (b) Co@P, N-C electrodes at various scan rates. GCD curves of (c) Co@N-C and (d) Co@P, N-C electrodes at different current densities.

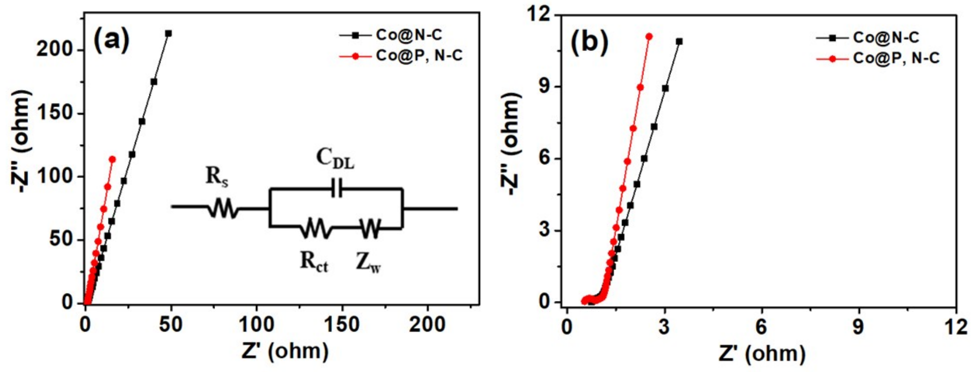

Fig. S23 EIS plots of the Co@N-C and Co@P, N-C electrodes at different magnifications.

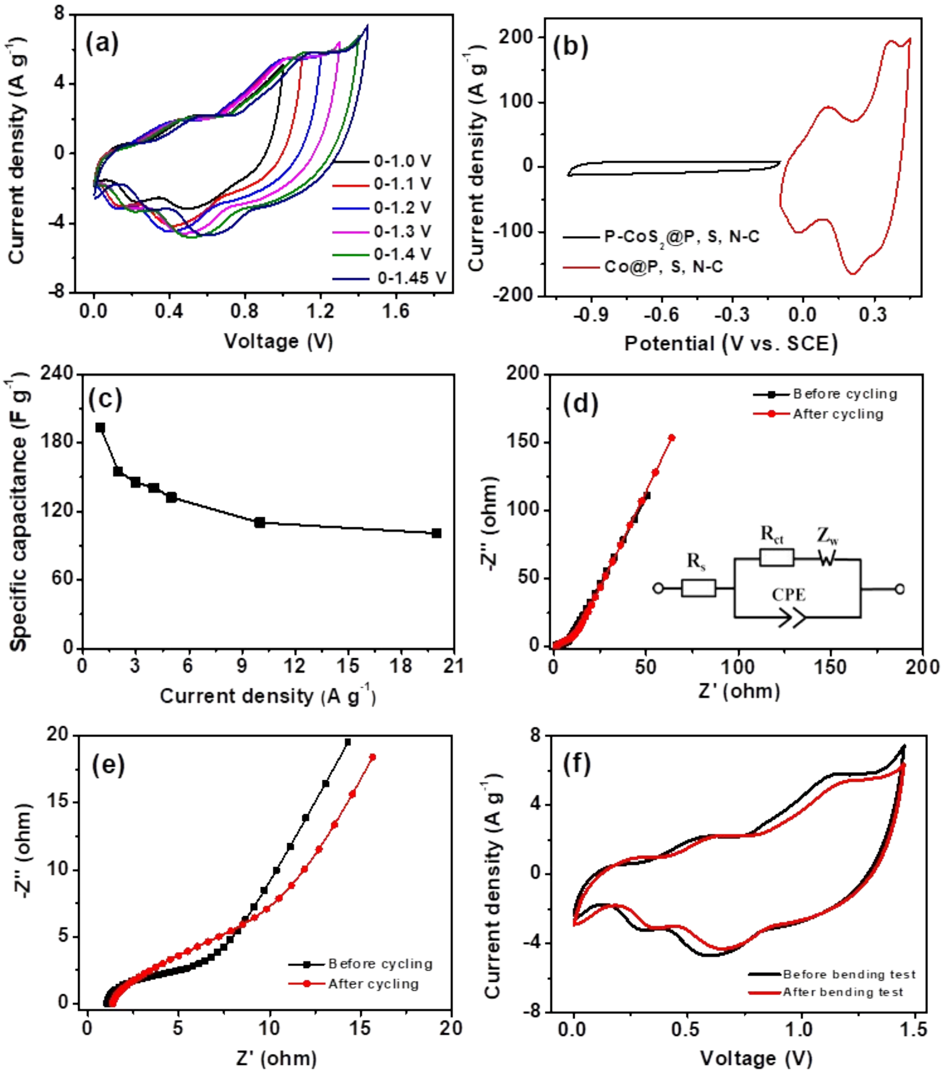

Fig. S24 (a) CV profiles of the as-constructed P-CoS$_2$@P, S, N-C//Co@P, N-C ASC device at a scan rate of 50 mV s^{-1} in different voltage windows; (b) CV curves of the P-CoS$_2$@P, S, N-C and Co@P, N-C electrodes in separate potential windows at a scan rate of 50 mV s^{-1}; (c) specific capacitance of the ASC device as a function of current density; (d, e) EIS plots of the ASC device at different magnifications; (f) CV curves of the ASC device before and after being flexed for 500 times at an angle range of 0−180°at a scan rate of 50 mV s^{-1}.

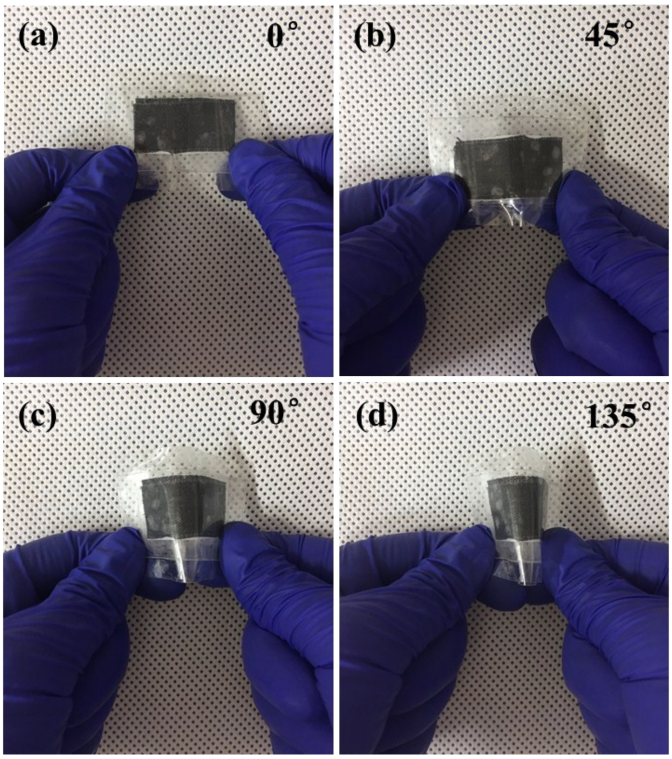

Fig. S25 Photographs of the fabricated ASC device under different bending conditions.

Table S1. Total energy values of the optimized structures for different systems.

System	E_o (eV)
CoS_2	–422.58703
OH-CoS_2	–433.15649
P-CoS_2	–423.41334
OH-P-CoS_2	–434.16983
P	–0.05893486
S	–0.059278944
OH^-	–7.09152660

Table S1 shows that the total energy of the P-CoS_2 system (–422.58703 eV) is lower compared with that of CoS_2 system (–423.41334). This result implies that the incorporation of P in CoS_2 is thermodynamically favored.

References

1. C. Guan, X. Liu, W. Ren, X. Li, C. Cheng and J. Wang, *Adv. Energy Mater.*, 2017, **7**, 1602391.
2. S. Liu, Y. Yin, K. S. Hui, K. N. Hui, S. C. Lee and S. C. Jun, *Adv. Sci.*, 2018, **5**, 1800733.
3. J. Hafner, *J. Comput. Chem.*, 2008, **29**, 2044-2078.
4. P. E. Blöchl, *Phys. Rev. B*, 1994, **50**, 17953.
5. J. Zhang, Y. Liu, C. Sun, P. Xi, S. Peng, D. Gao and D. Xue, *ACS Energy Letters*, 2018, **3**, 779-786.
6. J. Zhang, W. Xiao, P. Xi, S. Xi, Y. Du, D. Gao and J. Ding, *ACS Energy Letters*, 2017, **2**, 1022-1028.
7. S. Yang, L. Peng, P. Huang, X. Wang, Y. Sun, C. Cao and W. Song, *Angew. Chem. Int. Ed.*, 2016, **55**, 4016-4020.
8. X. Dong, H. Jin, R. Wang, J. Zhang, X. Feng, C. Yan, S. Chen, S. Wang, J. Wang and J. Lu, *Adv. Energy Mater.*, 2018, **8**, 1702695.